

PACS numbers: 42.55.Lt; 42.60.Lh
DOI: 10.1070/QE2003v033n12ABEH002552

Theoretical analysis of the mechanisms of influence of hydrogen additions on the emission parameters of a copper vapour laser

A.M. Boichenko, G.S. Evtushenko, O.V. Zhdaneev, S.I. Yakovlenko

Abstract. **A kinetic model of the active medium of a copper vapour laser with hydrogen additions is proposed. The model is tested using the available experimental data. Various points of view concerning the improvement of the emission parameters of the laser by adding hydrogen are analysed in detail. It is shown that the improvement of lasing parameters caused by the hydrogen addition is explained by different mechanisms. In the case of low pump-pulse repetition rates, the improvement is caused by an increase in the initial ground-state density of copper atoms and by quenching of the metastable states of copper atoms. When the pump-pulse repetition rate is high, the improvement is achieved due to a decrease in the prepulse electron concentration and temperature.**

Keywords: *copper vapour laser, kinetic model, hydrogen addition.*

1. Introduction

The addition of hydrogen into the active medium of a copper vapour laser substantially enhances the lasing efficiency under certain experimental conditions [1, 2]. The improvement of the emission parameters of metal vapour lasers containing hydrogen in small amounts was recently observed in many papers (see, for example, Refs [3 – 10]). At present, lasers containing small additions of hydrogen (a few percent) in a buffer gas are most efficient (1 % – 3 %), their average powers being 100 – 200 W [2]. The improvement of the parameters of a copper vapour laser caused by the hydrogen addition was observed in Refs [3, 4]. The improvement also occurs in CuBr vapour lasers [5 – 7] and CuCl lasers [8], although in this case the influence of hydrogen can be indirect, involving the formation of hydrogen halides. The kinetic models of copper vapour lasers with hydrogen additions were developed in papers [9 – 11].

A.M. Boichenko, S.I. Yakovlenko A.M. Prokhorov General Physics Institute, Russian Academy of Sciences, ul. Vavilova 38, 119991 Moscow, Russia; e-mail: kindep@kapella.gpi.ru;
G.S. Evtushenko, O.V. Zhdaneev Tomsk Polytechnical University, prosp. Lenina 30, 634034 Tomsk, Russia; Institute of Atmospheric Optics, Siberian Branch, Russian Academy of Sciences, prosp. Akademicheskii, 1, 634055 Tomsk, Russia

Received 9 December 2002; revision received 14 April 2003
Kvantovaya Elektronika **33** (12) 1047 – 1058 (2003)
Translated by M.N. Sapozhnikov

2. Description of the kinetic model

To determine the mechanism of influence of the hydrogen impurity on lasing parameters, we developed a kinetic model based on the model [12, 13] describing a pure copper vapour laser. Our model describes the time dependences of the volume-averaged level populations of a copper atom, molecular and atomic hydrogen, densities of copper and hydrogen ions, electron temperature, and laser emission intensities at the green and yellow lines of copper atoms, etc.

The model takes into account the nine states of the copper atom: Cu [Cu($4s^2S_{1/2}$), Cu($4s^2\,^2D_{5/2}$), Cu($4s^2\,^2D_{3/2}$), Cu($4p\,^2P_{3/2}$), Cu($4p\,^2P_{1/2}$), Cu($5s^2S_{1/2}$)], the ground state of the copper ion, and two states combining, respectively, three Cu^* [Cu($^4P^o$), Cu($^4D^o$), Cu($^4F^o$)] and four Cu^{**} [Cu($5p\,^2P_{3/2}$), Cu($5p\,^2P_{1/2}$), Cu($4d\,^2D_{5/2}$), Cu($4g\,^2D_{3/2}$)], closely spaced excited levels (see details in Refs [12, 13]). The ground and the first excited states (Ne and Ne^*) of the neon atom were taken into account, as well as the ground state of the Ne^+ ion. Also, the ground (H) and excited (H^*) atomic states of hydrogen and the H^+ and H^- ions were considered. In the molecular hydrogen, the ground state H_2 and the excited vibrational $v = 1 – 5$ levels were taken into account. In addition, molecular ions H_2^+ and H_3^+ were considered, as well as the ground state of the CuH molecule. Kinetic reactions involving hydrogen taken into account in the model are presented in Appendix.

Equations for the intensity $I(\lambda)$ of the 510.6-nm and 578.2-nm laser lines and expressions describing the time dependence of the electron temperature had the form similar to that presented in Refs [12, 13], with the corresponding additions accounting for the influence of hydrogen.

The balance equation for the gas temperature was not considered because the integration time of equations does not exceed the interpulse time during which the gas temperature is virtually constant.

The electron current density j in the active medium is described in the model by two methods. In the first case, the Kirchhoff equations for an electric circuit were solved self-consistently with the kinetic equations for concentrations of different reagents and the balance equation for the electron temperature. In the second case, the experimental time dependence of the current was directly used. This was especially important for testing the kinetic model by experimental data.

Nonstationary equations for the concentrations of different reagents, the balance equations for the electron temperature and (if necessary) the Kirchhoff equations for

an electric circuit (altogether 39 equations) were solved self-consistently using the PLASER software package [14, 15]. Altogether ~ 200 kinetic reactions were considered in the model.

3. Mechanisms of influence of the hydrogen impurity

Consider the mechanisms of influence of the hydrogen impurity on the operation of metal vapour lasers proposed in different papers:

3.1. No substantial improvement in the emission parameters of a copper vapour laser after the addition of hydrogen was reported in Ref. [1]. However, the authors of Ref. [1] were probably the first to conclude that the hydrogen impurity leads to an increase in the optimal laser-pulse repetition rate. The authors of this paper pointed out that the main mechanism of plasma recombination was ambipolar diffusion and the optimal pulse repetition rate was increased due to the enhancement of three-body recombination after the hydrogen addition.

3.2. According to Refs [12, 13, 16–19], a decrease in the prepulse concentration of electrons and copper atoms in the metastable state results in the increase in the output power and pulse repetition rate of metal vapour lasers. This can be achieved by the hydrogen addition: due to the high cross section for elastic collisions with hydrogen [3, 4], electrons are efficiently cooled in the interpulse time, resulting in a decrease in the concentration of copper atoms in the metastable state. The cooling of electrons causes in turn an increase in the recombination rate of positive copper ions, which reduces the prepulse electron concentration.

3.3. The prepulse electron concentration in the active medium of the laser can also decrease [5–7] due to the attachment of electrons to atomic hydrogen and the dissociative attachment of electrons to hydrogen molecules (especially to vibrationally excited molecules).

3.4. The improvement of the matching of a gas-discharge tube (GDT) with the excitation scheme allows the active medium to be excited more efficiently, providing thereby a higher lasing efficiency. According to Refs [4–7, 9, 10], such an improvement is achieved due to a lower initial conductivity of the GDT.

3.5. It was found in Refs [7, 20] that, after the addition of hydrogen into the active medium, the depletion of the ground state of copper during the excitation pulse decreased, while the ground-state population of copper recovered faster during the interpulse time, especially at the initial stage (for the first several microseconds). The increase in the recovery rate of the ground-state concentration of copper atoms will allow one to increase the energy output in the optimal regime. Note that mechanisms considered in paragraphs 3.3–3.5 were discussed in papers [5–7] as applied to CuBr lasers.

3.6. The improvement of the emission parameters of a copper vapour laser after the addition of hydrogen was explained in Ref. [10] by the rise in the ground-state concentration of copper atoms in the active medium due to the increase in the GDT wall temperature, which is probably caused by the increase in the energy supplied to the discharge. Note that this mechanism can result in an adverse positive feedback, when an increase in the supplied power leads to an increase in the wall temperature, thereby increasing the concentration of copper atoms. As a result, due to the increase in the collision frequency, the resistance of plasma increases, etc. and, eventually, this can lead to the quenching of lasing.

3.7. According to Ref. [10], due to an increase in the heat conduction of the active medium after the addition of hydrogen, the gas temperature on the GDT axis decreases. This reduces the concentration of copper atoms in metastable states (at lower laser levels), resulting in the enhancement of lasing. As for a change in the heat conduction of plasma after the addition of hydrogen, at present there is no consensus. Some researchers [10, 21] confirmed a change in the radial profile of the gas temperature, while other found that these changes are minimal [6]. Note that the improvement of the homogeneity of the radial distribution of the gas temperature is favourable for lasing because it reduces the heating of the active medium.

3.8. The reduction in the total output power at the hydrogen concentration above the optimal value is explained in Ref. [4] by the increase in energy losses during inelastic excitation and ionisation of molecular hydrogen. It was pointed out in Ref. [10] that the excess concentration of hydrogen reduced the concentration and temperature of electrons, which limits the population of the upper laser levels.

3.9. According to Refs [22, 23], the parameters of the laser improved with increasing the quenching rate of metastable copper atoms by vibrationally excited hydrogen molecules accompanied by the formation of the CuH molecule.

A detailed comparison of our theoretical calculations with experimental and theoretical data from Refs [9, 10], which report the most comprehensive data known to us, is presented in Section 5. Because the results of our simulation well agree with the data obtained in these papers, we used the laser parameters from Ref. [9] to study the mechanisms of influence of the hydrogen impurity on the kinetics of an active medium (Table 1).

Table 1. Parameters of the GDT [9, 10] used in simulations of the operation of lasers.

Reference	l/cm	d/cm	f/kHz	p_{Ne}/Torr	N_{H_2}/cm^{-3}
[9]	150	3.8	12	36	2×10^{15}
[10]	90	4	5	30	10^{15}

Note: l is the active medium length; d is the GDT diameter; f is the pump-pulse repetition rate; p_{Ne} is the neon pressure; N_{H_2} is the hydrogen concentration.

4. Analysis of the proposed assumptions

Let us analyse the above assumptions about the influence of the hydrogen addition on the kinetics of processes proceeding in the active medium. The numbering of assumptions analysed in Section 4 corresponds to that used in Section 3.

The estimate of the significance of various processes in calculations is considerably simplified by using reaction flows (see, for example, Ref. [24]). The reaction flow in the interval between instants t_1 and t_2 is defined as

$$F(t_1, t_2) = \int_{t_1}^{t_2} kN_1 \dots N_n \mathrm{d}t,$$

where k is the reaction rate and N_i are the concentrations of reagents involved in the reaction. The relations between the values of these functions give direct information on the role

of reactions in the production or disappearance of some reagent during a given time interval. The contribution of some reaction to the energy balance of electrons is determined by the product of the reaction flow by the energy transferred to electrons in an elementary event specified by this reaction.

4.1. The authors of Ref. [1] assume that the electron concentration decreases primarily due to ambipolar diffusion. According to calculations performed, for example, for the experimental conditions [9], the electron concentration is reduced mainly due to volume recombination rather than ambipolar diffusion. The relaxation of plasma in pulsed metal vapour lasers is determined by three-body recombination. This fact was pointed out long ago in papers on metal vapour lasers (see, for example, Refs [2, 25]). On the other hand, the authors of paper [1] report that the addition of atomic hydrogen is preferable than that of molecular hydrogen. According to our simulation, it is the dissociation and vibrational excitation of molecular hydrogen during the excitation pulse that mainly contribute to the cooling of electrons (see paragraph 4.8). The specific contribution of the elastic cooling of electrons by molecular and atomic hydrogen should be approximately the same. However, an increase in the laser pulse repetition rate after the hydrogen addition is indeed explained by a decrease in the electron density because of their more intense cooling. One can see from Fig. 1a that the presence of impurity hydrogen at the initial stage of an interpulse time causes a substantial increase in the rate of the electron temperature decay, which in turn results in a faster reduction of the electron concentration. This mechanism proves to be most significant at high pump-pulse repetition rates (low pulse repetition rates are considered in paragraph 4.6).

4.2. The authors of Ref. [4] proposed the mechanism of influence of hydrogen on the emission parameters of a copper vapour laser based on the fact that the cross section for elastic collisions of a hydrogen molecule with electrons is large. This should result, in the opinion of the authors of Ref. [1], in the improvement of the emission parameters due to cooling of electrons. However, the results of numerical calculations show that the influence of this mechanism on the kinetics of processes is negligible (Table 2).

Indeed, by comparing the reaction flows, one should bear in mind that, because of a small energy transferred in an elastic collision, the contribution of the elastic cooling reaction to the reduction of the electron temperature will be lower than that from other reactions, although the flow of this reaction is larger than flows of other reactions. The matter is that the contribution of an inelastic process to the balance equation for the electron temperature is $E_{ik}k_{ik}N_eN$, where E_{ik} is the energy transferred upon the inelastic collision of electrons (concentration N_e) with the atomic (molecular) component (concentration N) and k_{ik} is the reaction rate. The contribution from elastic collisions is $3\delta k_{el}(T_e - T_g)\times N_eN$, where $\delta = m_e/m$ is the ratio of the electron mass to the mass of an atom or a molecule (concentration N); k_{el} is the rate of the elastic process; and T_e and T_g are the electron and gas temperatures, respectively. One can see that the ratio of the contribution from elastic reactions to that from inelastic reactions is of the order of magnitude of the product of reaction flows by the factor $\delta(T_e - T_g)/E_{ik} \ll 1$.

Since we have already mentioned the question of a decrease in the prepulse electron concentration caused by cooling, let us discuss it in more detail. The reduction of the

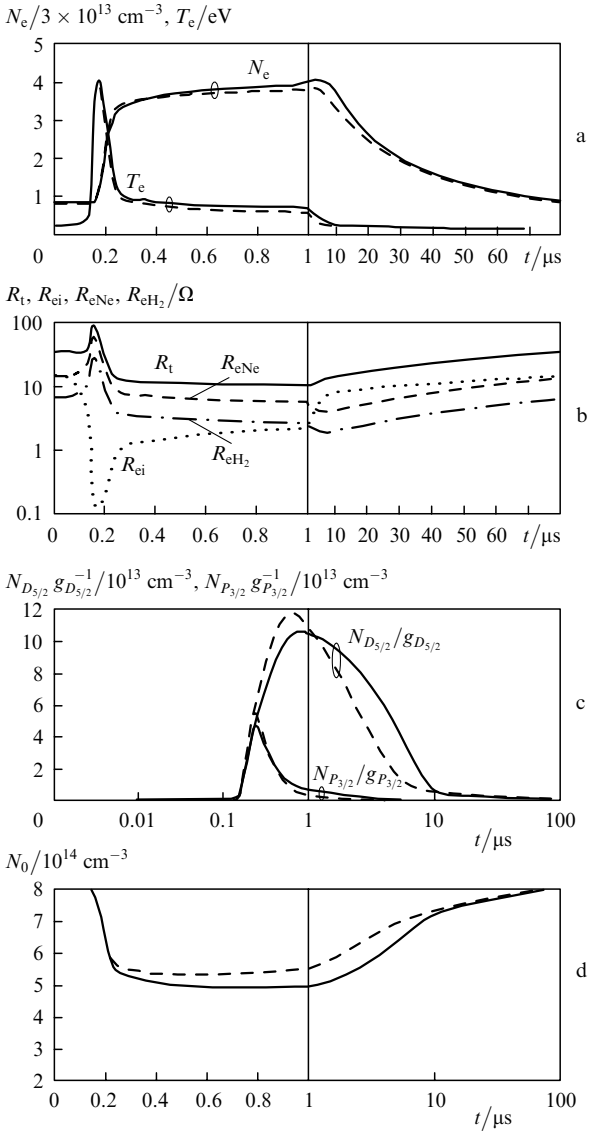

Figure 1. Time dependences of (a) the electron concentration and temperature during the excitation pulse and the interpulse time (solid curve: $N_{Cu} = 8\times10^{14}$ cm^{-3}, $N_{H_2} = 0$; dashed curve: $N_{Cu} = 10^{15}$ cm^{-3}, $N_{H_2} = 2\,\%$); (b) the plasma resistance (solid curve), the contribution of Coulomb electron–ion (dotted curve) and electron–atomic collisions (dashed curve), and the contribution of collisions with hydrogen (dot-and-dash curve) during the excitation pulse and the interpulse time for $N_{H_2} = 2\,\%$; (c) the level populations $N_{D_{5/2}}/g_{D_{5/2}}$ and $N_{P_{3/2}}/g_{P_{3/2}}$ during the excitation pulse (solid curves: $N_{Cu} = 8\times10^{14}$ cm^{-3}, $N_{H_2} = 0$, dashed curves: $N_{Cu} = 10^{15}$ cm^{-3}, $N_{H_2} = 2\,\%$); (d) the ground-state concentration of copper atoms during the excitation pulse and the interpulse time (solid curve: $N_{Cu} = 8\times10^{14}$ cm^{-3}, $N_{H_2} = 0$, dashed curve: $N_{Cu} = 10^{15}$ cm^{-3}, $N_{H_2} = 2\,\%$). The GDT parameters are presented in Table 1 and the values of plasma reagents used in calculations are given in Table 3 (for $N_{H_2} = 0$) and Table 4 (for $N_{H_2} = 2\,\%$, which corresponds to the initial concentration of molecular hydrogen in the mixture equal to 1.65×10^{15} cm^{-3}).

electron concentration, which favourably affects, according to paragraph 3.2, the lasing parameters, can also occur due to the reasons pointed out in paragraph 3.3. As mentioned above, studies [12, 13, 16, 18, 19] have shown that the prepulse electron concentration directly affects the laser parameters, in particular, the pulse repetition rate and the output energy that can be achieved. Therefore, it would be expected that a decrease in the prepulse electron concen-

Table 2. Reaction flows F (3 μs, 80 μs) of cooling and heating of electrons during the interpulse time in the case of a 2-% hydrogen impurity.

Reaction	Energy/eV	Reaction flows/cm^{-3}	Total reaction flows/cm^{-3}
$Ne^+ + 2e \rightarrow Ne^{**} + e$	3.1	$+1.41 \times 10^{13}$	$+1.41 \times 10^{13}$
Coulomb cooling	$-5.43 \times 10^{-4}(T_e - T_g)$	-6.272×10^{19}	-6.272×10^{19}
$Cu(P_{3/2}) + e \rightarrow Cu + e$	3.817	$+2.1 \times 10^{13}$	$+2.1 \times 10^{13}$
$Cu(P_{1/2}) + e \rightarrow Cu + e$	3.786	$+1.138 \times 10^{13}$	$+1.138 \times 10^{13}$
$Cu + e \rightarrow Cu(D_{5/2}) + e$ $Cu(D_{5/2}) + e \rightarrow Cu + e$	1.389	-5.139×10^{14} $+4.618 \times 10^{14}$	-5.17×10^{13}
$Cu + e \rightarrow Cu(D_{3/2}) + e$ $Cu(D_{3/2}) + e \rightarrow Cu + e$	1.642	-2.06×10^{14} $+3.38 \times 10^{14}$	$+1.32 \times 10^{14}$
$Cu(D_{5/2}) + e \rightarrow Cu(D_{3/2}) + e$ $Cu(D_{3/2}) + e \rightarrow Cu(D_{5/2}) + e$	0.253	-1.233×10^{15} $+1.122 \times 10^{15}$	-1.1×10^{14}
$Cu(P_{3/2}) + e \rightarrow Cu(P_{1/2}) + e$ $Cu(P_{1/2}) + e \rightarrow Cu(P_{3/2}) + e$	0.0313	$+4.395 \times 10^{15}$ -4.403×10^{15}	-8×10^{12}
$Cu^+ + 2e \rightarrow Cu^{**} + e$	1.58	$+6.542 \times 10^{13}$	$+6.542 \times 10^{13}$
Electron heat conductivity	–	-1.601×10^{14}	-1.601×10^{14}
$H^* + e = H + e$	10.2	$+2.724 \times 10^{12}$	$+2.724 \times 10^{12}$
$H_2 + e = H_2(v = 1) + e$ $H_2(v = 1) + e = H_2 + e$	0.5	-8.36×10^{14} $+9.465 \times 10^{14}$	$+1.105 \times 10^{14}$
$H_2(v = 1) + e = H_2(v = 2) + e$ $H_2(v = 2) + e = H_2(v = 1) + e$	0.5	-1.203×10^{14} $+1.479 \times 10^{14}$	$+2.76 \times 10^{13}$
$H_2 + e = H_2(v = 2) + e$	1	-1.394×10^{13}	-1.394×10^{13}
$H_2(v = 3) + e = H_2(v = 2) + e$	0.5	$+2.878 \times 10^{13}$	$+2.878 \times 10^{13}$
$H_2 + e = H_2 + e$	$-5.43 \times 10^{-4}(T_e - T_g)$	-1.07×10^{15}	-1.07×10^{15}

Note: The '+' and '−' signs denote heating (cooling) of electrons. To avoid completely the influence of the excitation pulse, the argument t_1 of the function F is set to be 3 μs and the end t_2 of the interpulse time corresponds to 80 μs ($f = 12$ kHz). The GDT parameters are presented in Table 1 and the initial reagents of the active medium in Table 4.

tration would produce a positive effect. However, the performed studies have shown (see also paragraph 4.5) that this effect becomes substantial only at high pump-pulse repetition rates. At low pulse repetition rates, the output energy increases mainly due to an increase in the copper concentration in the active medium (see paragraph 4.4). Moreover, if processes described in paragraph 4.4 did not occur after the addition of hydrogen, then the decrease in the prepulse electron concentration could not compensate for the negative effect of inelastic losses caused by hydrogen additions (see paragraph 4.8 and Fig. 1a).

4.3. The dissociative attachment of electrons to molecular hydrogen does not virtually improve the laser parameters. This reaction has a low efficiency because of its small cross section ($10^{-21} - 10^{-20}$ cm^2) and a rather high threshold (3.724 and 3.224 eV for the ground and the first vibrational level of the hydrogen molecule, respectively). The rate of reaction with atomic hydrogen is $\sim 10^{-28}$ cm^3 s^{-1}.

4.4. It was found in experimental papers [4–7] that after the addition of hydrogen to the active medium, the electric processes in the discharge circuit changed due to a change in the plasma conductivity (see also Fig. 1b, where the calculated plasma resistance is presented). In Ref. [4], this effect caused an increase in the power supplied to the discharge, resulting in the increase in the wall (gas) temperature and the copper concentration in the active medium of the GDT. As pointed out in Section 2, the balance equation for the gas temperature was not solved. However, it is clear that the gas temperature in the presence of hydrogen in the mixture will be higher than that without hydrogen due to, for example, the reactions of dissociation of hydrogen molecules by the electron impact and elastic cooling of the electrons by hydrogen molecules (see Appendix, reactions nos 9 and 53). Thus, the addition of hydrogen changes the initial ground-state concentration of copper atoms.

To verify this assumption, we increased the concentration of copper atoms in the active medium of the laser without the addition of hydrogen [but the GDT wall (and gas) temperature was not changed] and performed a series of calculations. As a result, we obtained even a greater increase in the output energy than upon the hydrogen addition (Tables 3 and 4). Therefore, it seems that the increase in the output power observed in experiments was achieved due to the increase in the GDT (gas) temperature and the concentration of copper atoms in the active medium.

The authors of Ref. [4] also performed experiments with a pure copper vapour laser in which the GDT temperature was forced to increase up to the temperature obtained after the hydrogen addition. However, an increase in the output power was only a few percent of its increase achieved after the addition of molecular hydrogen. Analysis of this fact shows that in the case of forced GDT heating, we not only change the concentration of copper, which was the aim of researchers in Ref. [4], but also increase simultaneously the level to which the electron temperature relaxes during the interpulse time, thereby determining the equilibrium concentration of copper atoms in the metastable state. Therefore, two competing processes will proceed simultaneously during forced heating of the gas: an increase in the copper density in the active medium and an increase in the

Table 3. Initial values of the plasma parameters and specific output energies per pulse at a pulse repetition rate of 12 kHz.

N_{H_2}/cm^{-3}	N_{Ne^+}/cm^{-3}	$N_{Cu^+}cm^{-3}$	$N_{D_{5/2}}/cm^{-3}$	$N_{D_{3/2}}/cm^{-3}$	N_{Cu}^{min}/cm^{-3}	N_{H^-}/cm^{-3}	N_{CuH}/cm^{-3}	N_{H_2} $(v=1)/$ cm^{-3}	N_{H_2} $(v=2)/$ cm^{-3}	T_e/eV	$E_{tot}/10^{-6}$ J cm^{-3}	$E_{510}/10^{-6}$ J cm^{-3}	$E_{578}/10^{-6}$ J cm^{-3}
0	6.25×10^{12}	1.96×10^{13}	7.54×10^{11}	1.06×10^{11}	4.91×10^{14}	–	–	–	–	0.171	3.00	2.14	0.86
1.65×10^{15}	6.13×10^{12}	1.90×10^{13}	7.38×10^{11}	1.01×10^{11}	5.07×10^{14}	1.63×10^{9}	7.98×10^{10}	7.70×10^{13}	2.90×10^{11}	0.170	2.95	2.10	0.85
3.30×10^{15}	5.96×10^{12}	1.79×10^{13}	6.31×10^{11}	8.66×10^{10}	5.20×10^{14}	2.01×10^{9}	1.19×10^{11}	1.39×10^{14}	4.77×10^{11}	0.165	2.92	2.09	0.833
1.65×10^{16}	4.25×10^{12}	1.20×10^{13}	1.94×10^{11}	2.10×10^{10}	5.73×10^{14}	2.36×10^{9}	6.35×10^{10}	2.80×10^{14}	4.08×10^{11}	0.1465	2.72	1.95	0.765
3.30×10^{16}	2.80×10^{12}	8.35×10^{12}	9.65×10^{10}	8.23×10^{9}	5.98×10^{14}	1.80×10^{9}	1.83×10^{10}	1.85×10^{14}	8.01×10^{10}	0.146	2.45	1.77	0.674
4.95×10^{16}	2.02×10^{12}	6.70×10^{12}	7.40×10^{10}	5.33×10^{9}	6.16×10^{14}	1.54×10^{9}	7.75×10^{9}	1.09×10^{14}	1.49×10^{10}	0.146	2.20	1.61	0.59

Note: Concentrations are $N_{Cu}=8\times10^{14}$ cm^{-3} and $N_H=10^{15}$ cm^{-3} for all cases when $N_{H_2}\neq0$. The initial values of the plasma reagents are calculated self-consistently (see Section 5), the GDT parameters are presented in Table 1. E_{tot} is the total specific output energy, E_{510} and E_{578} are the specific output energies at wavelengths of 510.6 and 578.2 nm; N_{Cu}^{min} is the minimal concentration of copper during the excitation pulse.

Table 4. Initial values of the plasma parameters and specific output energies per pulse at a pulse repetition rate of 12 kHz.

N_{H_2}/cm^{-3}	N_{Ne^+}/cm^{-3}	N_{Cu^+}/cm^{-3}	$N_{D_{5/2}}/cm^{-3}$	$N_{D_{3/2}}/cm^{-3}$	N_{Cu}^{min}/cm^{-3}	N_{H^-}/cm^{-3}	N_{CuH}/cm^{-3}	$N_{H_2}(v=1)/$ cm^{-3}	$N_{H_2}(v=2)/$ cm^{-3}	T_e/eV	$E_{tot}/10^{-6}$ J cm^{-3}	$E_{510}/10^{-6}$ J cm^{-3}	$E_{578}/10^{-6}$ J cm^{-3}
0	4.86×10^{12}	2.12×10^{13}	9.33×10^{11}	1.31×10^{11}	5.91×10^{14}	–	–	–	–	0.171	3.63	2.58	1.05
1.65×10^{15}	4.75×10^{12}	2.05×10^{13}	8.80×10^{11}	1.23×10^{11}	6.49×10^{14}	1.65×10^{9}	9.92×10^{10}	7.80×10^{13}	3.06×10^{11}	0.170	3.56	2.53	1.03
3.30×10^{15}	4.66×10^{12}	1.96×10^{13}	7.18×10^{11}	9.70×10^{10}	6.63×10^{14}	2.06×10^{9}	1.53×10^{11}	1.42×10^{14}	5.17×10^{11}	0.167	3.54	2.52	1.02
1.65×10^{16}	3.41×10^{12}	1.32×10^{13}	2.23×10^{11}	2.39×10^{10}	7.25×10^{14}	2.46×10^{9}	8.17×10^{10}	2.96×10^{14}	4.72×10^{11}	0.1465	3.31	2.37	0.942

Note: $N_{Cu}=10^{15}$ cm^{-3}, $N_H=10^{15}$ cm^{-3} (see note to Table 3).

prepulse population of the metastable level of copper atoms. Thus, we can conclude that the increase in the concentration of copper atoms in the metastable state does not result in a substantial increase in the output power in the absence of hydrogen additions.

Indeed, an increase in the concentration of copper atoms in the ground state caused by an increase in the energy supply (increase in the gas temperature) after adding hydrogen into the active medium is accompanied, according to our calculations, by a decrease in the prepulse concentration of copper atoms in the metastable state due to its quenching by vibrationally excited hydrogen molecules [in this case, the prepulse concentrations of metastable states of copper differ by 12 % – 14 % (for the 2 % hydrogen impurity), the total output energy increases by 18%, from 3.00×10^{-6} J cm^{-3} per pulse to 3.56×10^{-6} J cm^{-3} (see Tables 3 and 4 and Fig. 1c), and the lasing efficiency increases by 20 %, from 0.421 % up to 0.505 %).

Thus, according to our calculations, the output power was increased in experiments after the addition of hydrogen due to the increase in the gas temperature and, hence, in the copper concentration in the active medium along with a simultaneous reduction in the prepulse population of metastable levels due to their quenching by hydrogen molecules (see also paragraph 4.1).

4.5. The mechanisms of depletion are analysed in paragraphs 4.4, 4.6, and 4.8.

4.6. The authors of Ref. [6] observed a decrease in the depletion and a faster recovery of the prepulse concentration of copper atoms in the ground state after adding hydrogen. We obtained this effect in our numerical experiments as well. The main reaction flows changing the ground-state population of copper atoms are presented in Table 5 (see also Fig. 1d). One can see that the reaction flows decrease after adding hydrogen, which results in the increase in the minimal value to which the ground-state population of copper atoms decreases.

The hydrogen impurity affects indirectly the ground-state population of copper atoms by changing the electron concentration and temperature because it follows from Table 5 that reactions involving hydrogen do not affect substantially the ground-state population of copper atoms. One can also see from Table 5 that molecular hydrogen 'intercepts' the pump pulse energy, which is spent then for dissociation and excitation of the first vibrational levels of hydrogen. Therefore, a lower energy flux is spent for excitation of copper atoms than in the absence of hydrogen (see also paragraph 4.4).

4.7. To determine a change in the electron heat conductivity caused by the hydrogen addition, we performed a number of numerical experiments. We found that, despite a large total cross section for scattering electrons by molecular hydrogen, hydrogen does not produce a noticeable change in the electron heat conductivity because of its low content compared to a buffer gas (the electron heat conductivity changed less than by 1 % after the addition of 2% of hydrogen).

4.8. It is assumed in Ref. [1] that one of the possible negative factors of a change in the kinetics of a copper vapour laser after the addition of hydrogen can be the energy losses for inelastic processes of ionisation and excitation of molecular hydrogen. We analysed this hypothesis in detail and found that molecular hydrogen added into the active medium affects significantly the kinetics of processes during the excitation pulse. In particular, the reactions

$$H_2 + e \rightarrow H + H + e,$$

$$H_2 + e \rightarrow H_2(v=1) + e$$

(see Appendix) strongly affect the electron temperature during the first hundreds of nanoseconds (Table 6). In this case, the electron concentration also decreases (Fig. 1a), and, as the percent content of the hydrogen impurity is increased, the role of dissociation and excitation of the first vibrational levels of molecular hydrogen becomes more significant, resulting in a general change in kinetic processes proceeding in the active medium.

Table 5. Reaction flows F (0, 500 ns) of the depletion and recovery of the ground-state concentration of copper atoms during the excitation pulse.

Reaction	$N_{Cu} = 0.8 \times 10^{15}$ cm^{-3} (without H_2)		$N_{Cu} = 0.8 \times 10^{15}$ cm^{-3} (2 % H_2)		$N_{Cu} = 10^{15}$ cm^{-3} (2 % H_2)	
	Reaction flows/cm^{-3}	Total flows/cm^{-3}	Reaction flows/cm^{-3}	Total flows/cm^{-3}	Reaction flows/cm^{-3}	Total flows/cm^{-3}
$Cu + e \rightarrow Cu(P_{3/2}) + e$ $Cu(P_{3/2}) + e \rightarrow Cu + e$	-1.515×10^{14} $+6.751 \times 10^{13}$	-8.399×10^{13}	-1.402×10^{14} $+6.061 \times 10^{13}$	-7.959×10^{13}	-1.671×10^{14} $+6.689 \times 10^{13}$	-9.314×10^{13}
$Cu + e \rightarrow Cu(P_{1/2}) + e$ $Cu(P_{1/2}) + e \rightarrow Cu + e$	-7.232×10^{13} $+3.276 \times 10^{13}$	-3.956×10^{13}	-6.689×10^{13} $+2.946 \times 10^{13}$	-3.743×10^{13}	-7.977×10^{13} $+3.598 \times 10^{13}$	-4.379×10^{13}
$Cu + e \rightarrow Cu(D_{5/2}) + e$ $Cu(D_{5/2}) + e \rightarrow Cu + e$	-1.293×10^{14} $+3.494 \times 10^{13}$	-9.436×10^{13}	-1.229×10^{14} $+3.446 \times 10^{13}$	-8.844×10^{13}	-1.568×10^{14} $+4.553 \times 10^{13}$	-1.115×10^{14}
$Cu + e \rightarrow Cu(D_{3/2}) + e$ $Cu(D_{3/2}) + e \rightarrow Cu + e$	-1.137×10^{14} $+6.053 \times 10^{13}$	-5.317×10^{13}	-1.068×10^{14} $+5.852 \times 10^{13}$	-4.828×10^{13}	-1.351×10^{14} $+7.631 \times 10^{13}$	-5.879×10^{13}
$Cu + e \rightarrow Cu^* + e$ $Cu^* + e \rightarrow Cu + e$	-1.191×10^{13} $+8.66 \times 10^{10}$	-1.182×10^{13}	-1.107×10^{13} $+7.283 \times 10^{10}$	-1.1×10^{13}	-1.317×10^{13} $+8.643 \times 10^{10}$	-1.308×10^{13}
$Cu + e \rightarrow Cu^+ + 2e$	-1.916×10^{13}	-1.916×10^{13}	-1.842×10^{13}	-1.842×10^{13}	-2.135×10^{13}	-2.135×10^{13}
$Cu(D_{5/2}) + Cu \rightarrow Cu + Cu$	$+1.63 \times 10^{10}$	$+1.63 \times 10^{10}$	$+1.656 \times 10^{10}$	$+1.656 \times 10^{10}$	$+2.606 \times 10^{10}$	$+2.606 \times 10^{10}$
$Cu(D_{3/2}) + Cu \rightarrow Cu + Cu$	$+4.13 \times 10^{9}$	$+4.13 \times 10^{9}$	$+4.118 \times 10^{9}$	$+4.118 \times 10^{9}$	$+6.407 \times 10^{9}$	$+6.407 \times 10^{9}$
$Ne^* + Cu \rightarrow Cu^+ + Ne + e$	-3.612×10^{12}	-3.612×10^{12}	-3.712×10^{12}	-3.712×10^{12}	$+4.033 \times 10^{12}$	$+4.033 \times 10^{12}$
$Cu(P_{3/2}) \rightarrow Cu$	$+2.68712{:}1110^{12}$	$+2.68712{:}1110^{12}$	$+2.492 \times 10^{12}$	$+2.492 \times 10^{12}$	$+2.919 \times 10^{12}$	$+2.919 \times 10^{12}$
$Cu(P_{1/2}) \rightarrow Cu$	$+1.368 \times 10^{12}$	$+1.368 \times 10^{12}$	$+1.27 \times 10^{12}$	$+1.27 \times 10^{12}$	$+1.49 \times 10^{12}$	$+1.49 \times 10^{12}$
$NeCu^+ + e \rightarrow Cu + Ne$	$+5.53 \times 10^{10}$	$+5.53 \times 10^{10}$	$+5.09 \times 10^{10}$	$+5.09 \times 10^{10}$	$+5.793 \times 10^{10}$	$+5.793 \times 10^{10}$
$CuH + H_2 \rightarrow H_2(v = 3) + Cu$	–	–	$+7.934 \times 10^{10}$	$+7.934 \times 10^{10}$	$+9.898 \times 10^{10}$	$+9.898 \times 10^{10}$
$Cu(P_{1/2}) + H_2 \rightarrow Cu + H_2$	–	–	$+1.493 \times 10^{12}$	$+1.493 \times 10^{12}$	$+1.752 \times 10^{12}$	$+1.752 \times 10^{12}$
$Cu(P_{3/2}) + H_2 \rightarrow Cu + H_2$	–	–	$+2.892 \times 10^{12}$	$+2.892 \times 10^{12}$	$+3.391 \times 10^{12}$	$+3.391 \times 10^{12}$

Note: The choice of the arguments t_1 and t_2 of the function F is caused by the excitation pulse duration. The GDT parameters are presented in Table 1 and the initial concentrations of plasma reagents in Tables 3 and 4. The '+' and '−' signs denote the increase (decrease) in the copper concentration.

Table 6. Reaction flows F (0, 500 ns) of cooling and heating of electrons during the excitation pulse (see note to Table 5).

Reaction	$N_{Cu} = 0.8 \times 10^{15}$ cm^{-3} (without H_2)		$N_{Cu} = 10^{15}$ cm^{-3} (2 % H_2)	
	Reaction flows/cm^{-3}	Total flows/cm^{-3}	Reaction flows/cm^{-3}	Total flows/cm^{-3}
$Ne + e \rightarrow Ne^* + e$ $Ne^* + e \rightarrow Ne + e$	-1.756×10^{14} $+2.614 \times 10^{13}$	-1.494×10^{14}	-1.791×10^{14} $+2.007 \times 10^{13}$	-1.59×10^{14}
$Ne + e \rightarrow Ne^+ + 2e$	-4.157×10^{12}	-4.157×10^{12}	-4.295×10^{12}	-4.295×10^{12}
$Ne^* + e \rightarrow Ne^{**} + e$ $Ne^{**} + e \rightarrow Ne^* + e$	-2.926×10^{14} $+1.334 \times 10^{14}$	-1.592×10^{14}	-2.016×10^{14} $+8.392 \times 10^{13}$	-1.177×10^{14}
$Cu + e \rightarrow Cu(P_{3/2}) + e$ $Cu(P_{3/2}) + e \rightarrow Cu + e$	-1.459×10^{14} $+6.527 \times 10^{13}$	-8.063×10^{13}	-1.139×10^{14} $+4.076 \times 10^{13}$	-7.314×10^{13}
$Cu + e \rightarrow Cu(P_{1/2}) + e$ $Cu(P_{1/2}) + e \rightarrow Cu + e$	-6.962×10^{13} $+3.170 \times 10^{13}$	-3.792×10^{13}	-5.421×10^{13} $+1.990 \times 10^{13}$	-3.431×10^{13}
$Cu + e \rightarrow Cu(D_{5/2}) + e$	-1.301×10^{14}	-1.301×10^{14}	-9.005×10^{13}	-9.005×10^{13}
$Cu + e \rightarrow Cu(D_{3/2}) + e$	-1.132×10^{14}	-1.132×10^{14}	-7.586×10^{13}	-7.586×10^{13}
$Cu(D_{3/2}) + e \rightarrow Cu + e$	$+6.199 \times 10^{13}$	$+6.199 \times 10^{13}$	$+4.444 \times 10^{13}$	$+4.444 \times 10^{13}$
$Cu + e \rightarrow Cu^* + e$	-1.148×10^{13}	-1.148×10^{13}	-9.217×10^{12}	-9.217×10^{12}
$Cu + e \rightarrow Cu^+ + 2e$	-1.853×10^{13}	-1.853×10^{13}	-1.699×10^{13}	-1.699×10^{13}
$Cu(D_{5/2}) + e \rightarrow Cu^* + e$	-1.809×10^{13}	-1.809×10^{13}	-7.318×10^{12}	-7.318×10^{12}
$Cu(P_{3/2}) + e \rightarrow Cu^* + e$	-3.689×10^{13}	-3.689×10^{13}	-2.173×10^{13}	-2.173×10^{13}
$Cu(P_{3/2}) + e \rightarrow Cu(P_{1/2}) + e$ $Cu(P_{1/2}) + e \rightarrow Cu(P_{3/2}) + e$	$+1.366 \times 10^{16}$ -1.369×10^{16}	-3×10^{13}	$+8.531 \times 10^{15}$ -8.547×10^{15}	-1.6×10^{13}
$H_2 + e \rightarrow H + H + e$	–	–	-6.931×10^{13}	-6.931×10^{13}
$H_2 + e \rightarrow H_2^+ + 2e$	–	–	-1.044×10^{13}	-1.044×10^{13}
$H_2 + e \rightarrow H_2(v = 1) + e$	–	–	-6.407×10^{14}	-6.407×10^{14}

Note: The '+' and '−' signs denote heating (cooling) of electrons.

The electron temperature and the metastable-state population of copper atoms do not decrease substantially by the end of the interpulse time at low pulse repetition rates because electrons quench the excited vibrational levels of the hydrogen molecule. This slows down the rate of a decrease in the electron concentration, which adversely affects the recombination rate of the plasma. Thus, at low (of the order of 10 kHz) pump-pulse repetition rates, the prepulse electron concentration and temperature decrease insignificantly (approximately by 10 % – 15 %, see Fig. 1a). As the pump-pulse repetition rate is increased, a decrease in the prepulse electron concentration and temperature can lead, however, to positive effects (see the previous paragraph and also paragraph 4.5).

The intercept of the pump energy by hydrogen illustrated above (see also paragraph 4.6) adversely affects the parameters of a copper vapour laser. Nevertheless, the improvement of the laser parameters due to the effect described in paragraph 4.4 exceeds the negative action described above.

4.9. The authors of Ref. [22] proposed and studied the mechanism of quenching of the metastable state of copper atoms caused by the interaction with vibrationally excited hydrogen molecules. We analysed the influence of this process on the metastable-state population of copper atoms by calculating the reaction flows changing the metastable-state population of copper atoms. Table 7 presents the reaction flows for the $D_{5/2}$ level. Note that the quenching of the metastable level of copper atoms by vibrationally excited hydrogen molecules proves to be one of the most important processes affecting the level population, especially at the beginning of the interpulse time, which was pointed out earlier in Ref. [23].

This mechanism at low pump-pulse repetition rates is described in detail in paragraph 4.4.

Table 7. Reaction flows F (3 μs, 80 μs) of the decrease and increase in the population of the $D_{5/2}$ level of a copper atom during the interpulse time (see note to Table 2).

Reaction	Reaction flows/cm^{-3}	Total flows/cm^{-3}
$Cu + e \rightarrow Cu(D_{5/2}) + e$	$+4.618 \times 10^{14}$	-5.21×10^{13}
$Cu(D_{5/2}) + e \rightarrow Cu + e$	-5.139×10^{14}	
$Cu(D_{5/2}) + e \rightarrow Cu(P_{3/2}) + e$	-6.206×10^{10}	$+5.58 \times 10^{12}$
$Cu(P_{3/2}) + e \rightarrow Cu(D_{5/2}) + e$	$+5.643 \times 10^{12}$	
$Cu(D_{3/2}) + e \rightarrow Cu(D_{5/2}) + e$	$+1.122 \times 10^{15}$	-1.11×10^{14}
$Cu(D_{5/2}) + e \rightarrow Cu(D_{3/2}) + e$	-1.233×10^{15}	
$Cu^* + e \rightarrow Cu(D_{5/2}) + e$	$+7.525 \times 10^{10}$	$+6.418 \times 10^{10}$
$Cu(D_{5/2}) + e \rightarrow Cu^* + e$	-1.107×10^{10}	
$Cu(D_{5/2}) + e \rightarrow Cu^{**} + e$	-5.758×10^{6}	$+8.301 \times 10^{9}$
$Cu^{**} + e \rightarrow Cu(D_{5/2}) + e$	$+8.307 \times 10^{9}$	
$Cu(D_{3/2}) + Cu \rightarrow Cu(D_{5/2}) + Cu$	$+1.72 \times 10^{12}$	$+1.72 \times 10^{12}$
$Cu(D_{5/2}) + Cu \rightarrow Cu + Cu$	-2.35×10^{11}	-2.35×10^{11}
$Cu(P_{3/2}) \rightarrow Cu(D_{5/2})$	$+6.752 \times 10^{12}$	$+6.752 \times 10^{12}$
$Cu^{**} \rightarrow Cu(D_{5/2})$	$+7.468 \times 10^{12}$	$+7.468 \times 10^{12}$
$Cu(P_{3/2}) + h\nu \rightarrow Cu(D_{5/2}) + 2h\nu$	$+3.081 \times 10^{7}$	$+3.081 \times 10^{7}$
$Cu(D_{5/2}) + h\nu \rightarrow Cu(P_{3/2})$	-1.046×10^{9}	-1.046×10^{9}
$Cu(P_{3/2}) \rightarrow Cu(D_{5/2}) + h\nu$	$+1.385 \times 10^{9}$	$+1.385 \times 10^{9}$
$Cu(D_{5/2}) + H_2(v = 1) \rightarrow CuH + H$	-2.533×10^{13}	-2.533×10^{13}
$Cu(D_{5/2}) + H_2(v = 2) \rightarrow CuH + H$	-1.693×10^{12}	-1.693×10^{12}
$Cu(D_{5/2}) + H_2(v = 3) \rightarrow CuH + H$	-2.407×10^{11}	-2.407×10^{11}

Note: The '+' and '–' signs denote the increase (decrease) in the population of the $D_{5/2}$ level.

5. Testing of the model

The model was tested using experimental data obtained in Refs [9, 10]. These papers contain the most detailed results of theoretical and experimental studies of the influence of hydrogen additions on the parameters of a copper vapour laser.

We used in the calculations the experimental time dependence of the current flowing through a GDT during a excitation pulse. According to Refs [9, 10] and our calculations, the time dependence of the current changes insignificantly after adding hydrogen (at concentrations close to the optimal value of a few percent).

By comparing our calculations with the data obtained in Ref. [10], we used the initial concentration of copper atoms equal to that reported in Ref. [10]. The initial values of the rest of reagents were calculated in the model by iterations. We specified the initial concentrations of reagents and then calculated their values by the beginning of the next pulse. The iterations were stopped when the difference between the initial and final values was less than 1 %. This procedure is possible because of a weak time dependence of the current pulse shape after the addition of hydrogen.

5.1 Comparison with the results of Ref. [10]

The parameters of a GDT used in Ref. [10] and corresponding to the concentration of reagents in the active medium are presented in Table 1 and 8.

Table 8. Initial concentrations of the plasma reagents used in calculations for testing experiment [10].

Neon concentration	1.0×10^{17} cm^{-3}
Copper concentration	1.8×10^{15} cm^{-3}
Initial concentration of copper ions	9.85×10^{12} cm^{-3}
Initial population of the $D_{3/2}$ level	2.34×10^{10} cm^{-3}
Initial population of the $D_{5/2}$ level	2.43×10^{11} cm^{-3}
Initial concentration of vibrationally excited hydrogen for $v = 1$	1.02×10^{13} cm^{-3}
Initial concentration of vibrationally excited hydrogen for $v = 2$	2.68×10^{9} cm^{-3}
Initial concentration of CuH molecules	3.07×10^{9} cm^{-3}
Initial concentration of negative hydrogen ions	2.81×10^{8} cm^{-3}

Note: Except the ground-state concentrations of neon and copper, the parameters were calculated self-consistently using the model (see Section 2 and paragraph 5.1). The GDT parameters are presented in Table 1.

5.1.1 Voltage

The time dependence of the voltage in the absence of hydrogen well agree both with the experimental and calculated dependences presented in Ref. [10] (Fig. 2a). After the addition of 1% of H_2 into the mixture, the voltage across the GRT calculated using our model is approximately 1.5 times greater than that calculated in Ref. [10], although the shapes of the time dependences of the voltages

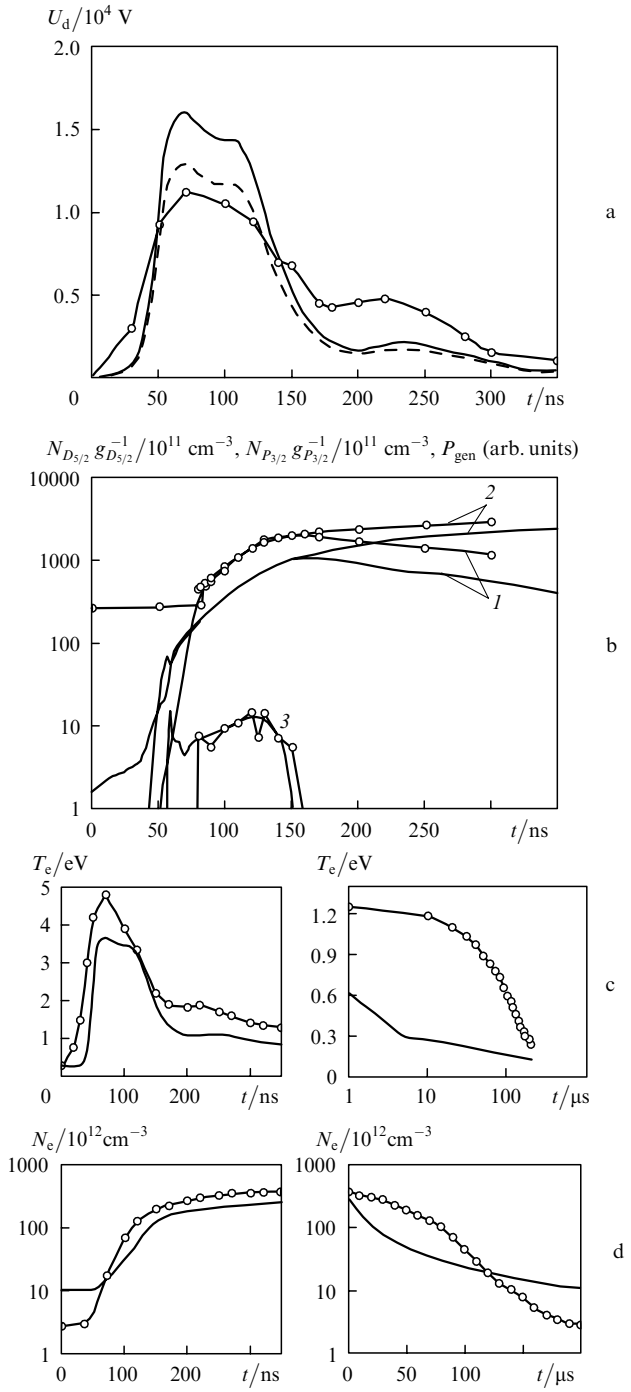

Figure 2. Time dependences of (a) the voltage across the GDT (circles are the experiment [10]; the results of our simulations: the dashed curve is calculated by neglecting the contribution of hydrogen to the plasma conduction; the solid curve is calculated taking this contribution into account); (b) the level populations $N_{P_{3/2}}/g_{P_{3/2}}$ (*1*) and $N_{D_{5/2}}/g_{D_{5/2}}$ (*2*) and the output pulse (*3*) (circles are the calculation [10] for the GDT axis, the solid curve is calculated in this paper); (c) the electron temperature during the excitation pulse and the interpulse time (circles are the calculation [10] for the GDT axis, the solid curve is calculated in this paper); (d) the electron concentration during the excitation pulse and the interpulse time (circles are the calculation [10] for the GDT axis, the solid curve is calculated in this paper). The GDT parameters and the values of plasma reagents used in calculations are presented in Tables 1 and 8, respectively.

are similar (Fig. 2a). Despite its low relative content in the active medium, hydrogen substantially increases the maximum resistance (Fig. 1b). Therefore, the above discrepancy can be explained by the fact that the authors of paper [10] probably did not take into account in calculations the influence of the hydrogen impurity on the conductivity.

5.1.2 Population of metastable levels

Our model predicts the lower prepulse population of the $D_{5/2}$ metastable level compared to that obtained in Ref. [10] (Fig. 2b). This is explained by a lower electron temperature at the end of the interpulse time in our calculations.

5.1.3 Electron temperature and concentration

We also compared the time dependences of the electron concentration and temperature (Figs 2c, d). As in calculations [10], the maximum concentration of electrons decreased with increasing content of the hydrogen impurity. According to our calculations, there exists a time delay in the onset of the rise of the electron concentration with time (Fig. 2d). However, unlike the results obtained in Ref. [10], our model did not predict any increase in the time delay with increasing the content of hydrogen in the active medium. A comparison of the time dependences of the electron temperature shows that the maximum electron temperature obtained in our calculations was lower (Fig. 2c). In addition, the electron temperature in Ref. [10] relaxed approximately to the same level both in the presence and absence of hydrogen. This is not quite clear because the initial populations of metastable levels were substantially different (the prepulse metastable-state concentration of copper atoms in the presence of the impurity hydrogen was twice as large as that for the 1-% addition of hydrogen). The time dependences of the electron temperatures during the interpulse time were also different.

Our calculations gave a distinct separation of the relaxation period into two stages: the electron temperature sharply decreased for the first several microseconds and then slowly decreased during the rest of the interpulse time. This is typical of a copper vapour laser [2, 25, 26]. At the same time, the opposite situation was observed in Ref. [10]: first the electron temperature slowly decreased and then it was strongly decreased at the end of the interpulse time (Fig. 2c).

The authors of paper [10] reported that the prepulse electron concentration increased after the addition of hydrogen. Therefore, according to Ref. [10], the addition of hydrogen leads to the increase in the concentrations of both metastable states and electrons, which deteriorates the prepulse conditions and contradicts our calculations.

5.2 Comparison with the results obtained by the group of Piper [9]

The time dependences of the ground-state concentration of copper atoms were compared (Fig. 3a) by taking the initial concentration of copper in the calculations equal to 10^{15} cm^{-3}. This value was determined by the fact that the ratio of the gas temperature to the GDT wall temperature T_g/T_{gw} was $\sim 1.3 - 1.5$ (the field temperature was calculated using the expression from Ref. [27]) and using the near-wall concentration of copper reported in Ref. [9]. For the initial copper density equal to 10^{15} cm^{-3}, rather good agreement with experimental output powers was also observed (Table 9).

The time dependence of the electron concentration predicted by our model differs from that reported in Ref. [9] as follows. The prepulse electron concentration

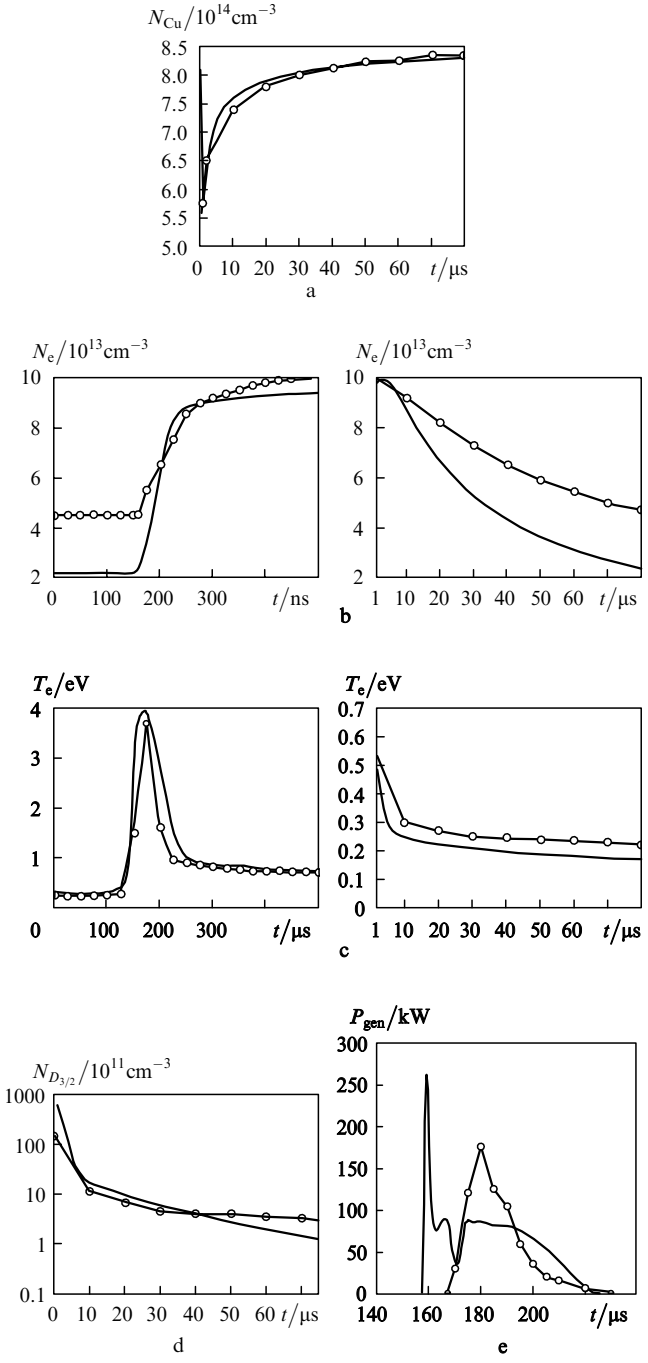

Figure 3. Time dependences of (a) the ground-state concentration of copper atoms during the excitation pulse and the interpulse time (circles are the calculation of the copper concentration at the GDT axis [9], the solid curve are calculations performed in this paper and normalised to the data [9]; $N_{Cu} = 0.83 \times 10^{15}$ cm^{-3} in calculations [9] and $N_{Cu} = 10^{15}$ cm^{-3} in our calculation, see paragraph 5.2); (b) the electron concentration during the excitation pulse and the interpulse time (circles are the electron concentration calculated at the GDT axis [9], the solid curve is calculated in this paper); (c) the electron temperature during the excitation pulse and the interpulse time (circles are the electron temperature at the GDT axis [9], the solid curve is our simulation); (d) the population of the $D_{3/2}$ level during the interpulse time (circles are the concentration of copper atoms in the $D_{3/2}$ state calculated at the GDT axis [9], the solid curve is calculated in this paper); (e) the laser pulse (circles are the laser pulse calculated at the GDT axis [9], the solid curve is calculated in this paper). The GDT parameters and the values of plasma reagents used in calculations are presented in Tables 1 and 4, respectively.

Table 9. Comparison of calculated laser output powers with experimental results [9].

Hydrogen content (%)	Experiment	Model		
	P/W	P/W	$P_{510.6}$/W	$P_{578.2}$/W
Absent	59.6	61.04	43.48	17.56
2	67.2	70.83	50.42	20.41

Note: The GDT parameters are presented in Table 1 and the concentrations of reagents in the active medium in Tables 3 and 4. The prepulse ground-state concentration of copper atoms used in calculations for pure neon and the 2% hydrogen impurity was 8×10^{14} and 10^{15} cm^{-3}, respectively (see paragraphs 3.4 and 5.2); P is the total output power, $P_{510.6}$ is the output power at 510.6 nm, and $P_{578.2}$ is the output power at 578.2 nm.

obtained in our calculations is approximately half as much and its maximum value achieved during the laser pulse is lower by 5%. Our calculations predict a greater rate of the electron concentration decrease during the interpulse time than in paper [9] (Fig. 3b).

The electron temperature during the excitation pulse is close to that obtained in Ref. [9]. The time dependence of the electron temperature during the interpulse time is similar to that obtained in Ref. [9]; however, the electron temperature is lower (Fig. 3c).

We also observed good agreement between the time dependences of populations of the ground-state and $D_{3/2}$ metastable levels. However, because of a higher concentration of copper in the active medium in Ref. [9], the time dependence curve for the ground-state population predicted by our model lies higher than that calculated in Ref. [9] (Figs 3a, d).

By comparing the laser pulses, note that the pulse predicted by our model has a more distinct vibrational structure at the beginning of lasing (Fig. 3e).

6. Pump pulses with a high pulse repetition rate

At low pump-pulse repetition rates, a positive effect of the reduction of the prepulse concentrations of electrons and copper atoms in the metastable state is reduced by the loss of the pump energy spent for the dissociation and excitation of the first vibrational levels of the hydrogen molecule (paragraph 4.8). However, it is the use of hydrogen in experimental papers [28–30] with a copper vapour laser that allowed the achievement of high pulse repetition rates. Although copper bromide vapour lasers were studied in Refs [29, 30], mechanisms revealed for the case of pure copper with hydrogen additions can operate in copper bromide vapour lasers as well. When the shape of the pump current pulse is invariable, the output energy increases after the addition of hydrogen even for the constant ground-state concentration of copper atoms, the increase in the output energy being greater for a pulse repetition rate of 100 kHz (Tables 10 and 11). Of course, the amplitude and shape of the current pulse in real experiments will change somewhat with increasing the pump-pulse repetition rate; however, it is rather difficult to take such changes into account in simulations because they depend on specific experimental conditions. In addition (see Sections 3 and 4), the gas temperature and other parameters can also change. The consideration of all these factors would result in a substantial complication of the model, especially as the experimental data are rather scarce and give no information on the magnitude of these changes in lasers with hydrogen

Table 10. Initial values of the plasma parameters and the specific output power per pulse at a pulse repetition rate of 50 kHz.

N_{H_2}/cm^{-3}	N_{Ne^+}/cm^{-3}	N_{Cu^+}/cm^{-3}	$N_{D_{5/2}}/cm^{-3}$	$N_{D_{3/2}}/cm^{-3}$	N_{H^-}/cm^{-3}	N_{CuH}/cm^{-3}	$N_{H_2}(v=1)/cm^{-3}$	$N_{H_2}(v=2)/cm^{-3}$	T_e/eV	$E_{tot}/10^{-6}$ J cm^{-3}	$E_{510}/10^{-6}$ J cm^{-3}	$E_{578}/10^{-6}$ J cm^{-3}
0	4×10^{12}	7.31×10^{13}	3.62×10^{12}	6.94×10^{11}	–	–	–	–	0.218	1.96	1.49	0.47
3.3×10^{15}	4.02×10^{12}	6.95×10^{13}	3.53×10^{12}	6.92×10^{11}	1.48×10^{10}	3.66×10^{12}	4.4×10^{14}	8.75×10^{12}	0.222	1.92	1.46	0.46
1.65×10^{16}	4×10^{12}	5.15×10^{13}	1.75×10^{12}	3.17×10^{11}	2.8×10^{10}	4.02×10^{12}	1.42×10^{15}	1.87×10^{13}	0.201	2.14	1.61	0.53
3.3×10^{16}	3.7×10^{12}	3.8×10^{13}	7.75×10^{11}	1.15×10^{11}	2.18×10^{10}	2.2×10^{12}	1.65×10^{15}	2.04×10^{13}	0.173	2.07	1.55	0.52
4.95×10^{16}	3.39×10^{12}	2.92×10^{13}	3.96×10^{11}	5.08×10^{10}	1.55×10^{10}	1×10^{12}	1.5×10^{15}	8.47×10^{12}	0.165	1.96	1.47	0.49

Note: Concentrations are $N_{Cu}=8\times10^{14}$ cm^{-3} and $N_H=10^{15}$ cm^{-3} (see note to Table 3).

Table 11. Initial values of the plasma parameters and the specific output power per pulse at a pulse repetition rate of 100 kHz.

N_{H_2}/cm^{-3}	N_{Ne^+}/cm^{-3}	N_{Cu^+}/cm^{-3}	$N_{D_{5/2}}/cm^{-3}$	$N_{D_{3/2}}/cm^{-3}$	N_{H^-}/cm^{-3}	N_{CuH}/cm^{-3}	$N_{H_2}(v=1)/cm^{-3}$	$N_{H_2}(v=2)/cm^{-3}$	T_e/eV	$E_{tot}/10^{-6}$ J cm^{-3}	$E_{510}/10^{-6}$ J cm^{-3}	$E_{578}/10^{-6}$ J cm^{-3}
0	4.5×10^{11}	1.25×10^{14}	7.14×10^{12}	1.54×10^{12}	–	–	–	–	0.21	5.83	5.83	0
1.65×10^{16}	1.19×10^{12}	9.05×10^{13}	5.5×10^{12}	1.1×10^{12}	7.6×10^{10}	2.82×10^{13}	2.33×10^{15}	7.05×10^{13}	0.211	1.17	0.966	0.204
3.3×10^{16}	1.74×10^{12}	6.95×10^{13}	2.22×10^{12}	4.12×10^{11}	7×10^{10}	1.75×10^{13}	3.2×10^{15}	7.5×10^{13}	0.202	1.4	1.13	0.266
4.95×10^{16}	1.92×10^{12}	5.45×10^{13}	1.12×10^{12}	1.85×10^{11}	5.37×10^{10}	1.01×10^{13}	3.26×10^{15}	5.06×10^{13}	0.185	1.43	1.15	0.28

Note: Concentrations are $N_{Cu}=8\times10^{14}$ cm^{-3} and $N_H=10^{15}$ cm^{-3} (see note to Table 3).

additions. In this case, the theory can give an inadequate description of the real situation. In addition, even all the above factors were taken into account in the model, this would only complicated the understanding of the situation (because of a great number of factors). For this reason, the current pulse was assumed invariable in calculations; however, the results presented in Table 10 and 11 demonstrate the possibility of a substantial improvement of the emission parameters of the laser.

7. Conclusions

We have developed a detailed kinetic model of the active $Ne-Cu-H_2$ medium of copper vapour lasers to study the influence of additions of hydrogen into the medium on the laser parameters and compared it with the experimental data available.

Our analysis has shown that the increase in the output power of lasers after adding molecular hydrogen is probably explained by different mechanisms at low and high pulse repetition rates.

At high pulse repetition rates ($f \gg 10$ kHz), the output power can increase due to decreasing prepulse concentrations of electrons and atoms in the metastable state, as well as due to the increase in the rate of recovery of the ground-state concentration of copper atoms.

At low pulse repetition rates ($f \sim 10$ kHz), the above mechanisms become insufficient. The output power increases due to the increase in the concentration of copper atoms in the active medium caused by the heating of the GDT after the addition of hydrogen and a simultaneous decrease in the prepulse concentration of metastable states of copper atoms quenched by vibrationally excited hydrogen molecules. In addition, after the introduction of hydrogen into the active medium, the current flowing through a GDT during the interpulse time decreases, which accelerates relaxation processes proceeding in the plasma. Note also that the addition of hydrogen causes some adverse effects. These are the greater consumption of energy deposited to the plasma during the excitation pulse for the dissociation and vibrational excitation of molecular hydrogen, as well as some slowing down of the plasma relaxation for the interpulse time due to the energy release in the electron component during thermalisation of vibrationally excited hydrogen molecules.

Appendix

Table 12. Kinetic processes involving atomic and molecular hydrogen (n is the number of reagents involved in the reaction).

No.	Reaction	Reaction rate/cm$^{3(n-1)}$ s^{-1}	Contribution to the electron temperature/eV	References
1	$H+e\rightarrow H^++2e$	$2\times10^{-8}\exp(-13.6/T_e)$	−13.6	[31]
2	$H^*+e\rightarrow H^++2e$	$4\times10^{-5}/T_e^3\exp(-3.4/T_e)$	−3.4	[32]
3	$H^++2e\rightarrow H^*+e$	$5.4\times10^{-27}T_e^{-9/2}$	3.4	[32]
4	$H+e\rightarrow H^*+e$	$2\times10^{-8}\exp(-10.2/T_e)$	−10.2	[33]
5	$H^*+e\rightarrow H+e$	2×10^{-8}	10.2	[32]
6	$H_2^++2e\rightarrow 2H+e$	$5.4\times10^{-27}T_e^{-9/2}$	4.4	[31]
7	$H_2^++H_2\rightarrow H_3^++H$	2×10^{-9}	–	[34]
8	$H_3^++e\rightarrow H_2+H$	$1\times10^{-7}T_e^{-1/2}$	$-1.5T_e$	[35]
9	$H_2+e\rightarrow 2H+e$	$2\times10^{-8}\exp(-8.8/T_e)$	−8.8	[32]
10	$H_2+e\rightarrow H_2^++2e$	$2\times10^{-8}\exp(-15.4/T_e)$	−15.4	[29]
11	$2H+H_2\rightarrow H_2+H_2$	$8.59\times10^{-34}T_g^{-0.61}$	–	[36]

(*continued on the next page*)

No.	Reaction	Reaction rate/$cm^{3(n-1)}\ s^{-1}$	Contribution to the electron temperature/eV	References
12	$2H + H \rightarrow H_2 + H$	$4.70 \times 10^{-33} T_g^{-0.95}$	–	[36]
13	$H^- + H \rightarrow H_2 + e$	1.3×10^{-9}	–	[31]
14	$H_2^+ + H_2 \rightarrow H_2^+ + 2H$	1.5×10^{-9}	–	[37]
15	$H_2^+ + e \rightarrow 2H$	$5.34 \times 10^{-8} T_e^{-0.4}$	$-1.5T_e$	[35]
16	$2H + Ne \rightarrow H_2 + Ne$	3×10^{-33}	–	[34]
17	$H_2\ (v = 1) + H \rightarrow H_2 + H$	$3.09 \times 10^{-11} \exp(-0.1205/T_g)$	–	[38, 39]
18	$H_2\ (v = 2) + H \rightarrow H_2\ (v = 1) + H$	$2.06 \times 10^{-10} \exp(-0.1205/T_g)$	–	[38, 39]
19	$H_2\ (v = 3) + H \rightarrow H_2\ (v = 2) + H$	$8.76 \times 10^{-10} \exp(-0.1205/T_g)$	–	[38, 39]
20	$H_2\ (v = 2) + H \rightarrow H_2 + H$	$1.53 \times 10^{-10} \exp(-0.1205/T_g)$	–	[38, 39]
21	$H_2\ (v = 3) + H \rightarrow H_2 + H$	$3.81 \times 10^{-10} \exp(-0.1205/T_g)$	–	[38, 39]
22	$H_2\ (v = 3) + H \rightarrow H_2\ (v = 1) + H$	$5.05 \times 10^{-10} \exp(-0.1205/T_g)$	–	[38, 39]
23	$H_2\ (v = 1) + H_2 \rightarrow H_2 + H_2$	$7.85 \times 10^{-10} T_g^{-4.3}$	–	[38, 39]
24	$H_2\ (v = 2) + H_2 \rightarrow H_2\ (v = 1) + H_2$	$2.62 \times 10^{-9} T_g^{-4.3}$	–	[38, 39]
25	$H_2\ (v = 3) + H_2 \rightarrow H_2\ (v = 2) + H_2$	$8.50 \times 10^{-9} T_g^{-4.3}$	–	[38, 39]
26	$H_2\ (v = 4) + H_2 \rightarrow H_2\ (v = 3) + H_2$	$2.06 \times 10^{-9} \exp(-0.1205/T_g)$	–	[38, 39]
27	$H_2\ (v = 5) + H_2 \rightarrow H_2\ (v = 4) + H_2$	$4.12 \times 10^{-9} \exp(-0.1205/T_g)$	–	[38, 39]
28	$H_2\ (v = 4) + H \rightarrow H_2 + H$	$1.03 \times 10^{-9} \exp(-0.1205/T_g)$	–	[38, 39]
29	$H_2\ (v = 4) + H \rightarrow H_2\ (v = 1) + H$	$0.99 \times 10^{-9} \exp(-0.1205/T_g)$	–	[38, 39]
30	$H_2\ (v = 4) + H \rightarrow H_2\ (v = 2) + H$	$1.5 \times 10^{-9} \exp(-0.1205/T_g)$	–	[38, 39]
31	$H_2\ (v = 5) + H \rightarrow H_2 + H$	$3.60 \times 10^{-10} \exp(-0.1205/T_g)$	–	[38, 39]
32	$H_2\ (v = 5) + H \rightarrow H_2(v = 1) + H$	$1.22 \times 10^{-9} \exp(-0.1205/T_g)$	–	[38, 39]
33	$H_2\ (v = 5) + H \rightarrow H_2(v = 2) + H$	$1.74 \times 10^{-9} \exp(-0.1205/T_g)$	–	[38, 39]
34	$H_2\ (v = 5) + H \rightarrow H_2(v = 3) + H$	$2.41 \times 10^{-9} \exp(-0.1205/T_g)$	–	[38, 39]
35	$H_2\ (v = 4) + H_2 \rightarrow H_2(v = 3) + H_2$	$1.96 \times 10^{-9} T_g^{-4.3}$	–	[38, 39]
36	$H_2\ (v = 5) + H_2 \rightarrow H_2(v = 4) + H_2$	$4.58 \times 10^{-8} T_g^{-4.3}$	–	[38, 39]
37	$H_2\ (v = 1) + H_2\ (v = 1) \rightarrow H_2(v = 2) + H_2$	7.6×10^{-13}	–	[38]
38	$H_2\ (v = 1) + H_2\ (v = 2) \rightarrow H_2(v = 3) + H_2$	1.1×10^{-12}	–	[38]
39	$H_2\ (v = 1) + H_2\ (v = 3) \rightarrow H_2(v = 4) + H_2$	8.4×10^{-13}	–	[38]
40	$H_2\ (v = 1) + H_2\ (v = 4) \rightarrow H_2(v = 5) + H_2$	1.1×10^{-12}	–	[38]
41	$H_2 + e \rightarrow H_2\ (v = 1) + e$	*	−0.5	[40]
42	$H_2\ (v = 1) + e \rightarrow H_2 + e$	*	0.5	[40]
43	$H_2\ (v = 1) + e \rightarrow H_2\ (v = 2) + e$	*	−0.5	[40]
44	$H_2 + e \rightarrow H_2\ (v = 2) + e$	*	−1	[40]
45	$H_2\ (v = 2) + e \rightarrow H_2 + e$	*	−1	[40]
46	$H_2\ (v = 2) + e \rightarrow H_2\ (v = 3) + e$	*	−0.5	[40]
47	$H_2 + e \rightarrow H_2\ (v = 3) + e$	*	−1.5	[38]
48	$H_2\ (v = 3) + e \rightarrow H_2 + e$	*	1.5	[42]
49	$H_2\ (v = 2) + e \rightarrow H_2\ (v = 1) + e$	3×10^{-9}	0.5	[38]
50	$H_2\ (v = 3) + e \rightarrow H_2\ (v = 2) + e$	5×10^{-9}	0.5	[38]
51	$H_2\ (v = 4) + e \rightarrow H_2\ (v = 3) + e$	5.5×10^{-9}	0.5	[38]
52	$H_2\ (v = 5) + e \rightarrow H_2\ (v = 4) + e$	5.5×10^{-9}	0.5	[38]
53	$H_2 + e \rightarrow H_2 + e$	*	$-5.43 \times 10^{-4}(T_e - T_g)$	[40]
54	$H + 2e \rightarrow H^- + e$	$3.31 \times 10^{-28} T_e^{-1}$	−0.754	[40]
55	$H^- + e \rightarrow H + 2e$	$10^{-6} \exp(-0.754/T_e) T_e^{0.5}$	0.754	[40]
56	$H_2 + e \rightarrow H^- + H$	*	−3.724	[41]
57	$H_2\ (v = 1) + e \rightarrow H^- + H$	*	−3.224	[41]
58	$H_2\ (v = 2) + e \rightarrow H^- + H$	*	−2.724	[41]
59	$H_2\ (v = 3) + e \rightarrow H^- + H$	*	−2.224	[41]
60	$H_2\ (v = 4) + e \rightarrow H^- + H$	*	−1.724	[41]
61	$Cu\ (D_{3/2}) + H_2\ (v = 1) \rightarrow CuH + H$	2×10^{-10}	–	[22, 23]
62	$Cu\ (D_{5/2}) + H_2\ (v = 1) \rightarrow CuH + H$	2×10^{-10}	–	[22, 23]
63	$Cu\ (D_{3/2}) + H_2\ (v = 2) \rightarrow CuH + H$	2×10^{-10}	–	[22, 23]
64	$Cu\ (D_{5/2}) + H_2\ (v = 2) \rightarrow CuH + H$	2×10^{-10}	–	[22, 23]
65	$Cu\ (D_{3/2}) + H_2\ (v = 3) \rightarrow CuH + H$	2×10^{-10}	–	[22, 23]
66	$Cu\ (D_{5/2}) + H_2\ (v = 3) \rightarrow CuH + H$	2×10^{-10}	–	[22, 23]

(*continued on the next page*)

No.	Reaction	Reaction rate/$cm^{3(n-1)}$ s^{-1}	Contribution to the electron temperature/eV	References
69	$CuH + H \rightarrow H_2(v = 3) + Cu$	2×10^{-10}	–	[22, 23]
70	$Cu(P_{1/2}) + H_2 \rightarrow Cu + H_2$	10^{-10}	–	Estimate
71	$Cu(P_{3/2}) + H_2 \rightarrow Cu + H_2$	10^{-10}	–	Estimate
72	$Cu^+ + H^+ + Ne \rightarrow Cu + H + Ne$	$1.28 \times 7.01 \times 10^{-31}/T_g^3$	–	[42]
73	$Ne^+ + H^- + Ne \rightarrow Ne + H + Ne$	$1.34 \times 7.01 \times 10^{-31}/T_g^3$	–	[42]
74	$H^+ + H^- + Ne \rightarrow H + H + Ne$	$2.05 \times 7.01 \times 10^{-31}/T_g^3$	–	[42]
75	Ambipolar diffusion H^+	$11.1 \times (2.7 \times 10^{19}/[Ne])(0.026/T_g)$ **	–	[43]
76	Ambipolar diffusion H_2^+	$7.5 \times (2.7 \times 10^{19}/[Ne])(0.026/T_g)$ **	–	[43]

Note. Temperatures T_e and T_g in the expressions for reaction rates are measured in electron-volts; * the reaction rate was calculated using the cross sections taken from the corresponding papers and assuming the Maxwell distribution of the electron energy; ** this expression was used to calculate the dependence of the mobility of ions on the concentration of Ne and T_g for estimating the time of ambipolar diffusion.

References

1. Bokhan P.A., Silant'ev V.I., Solomonov V.I. *Kvantovaya Elektron.*, **7**, 1264 (1980) [*Sov. J. Quantum Electron.*, **10**, 724 (1980)].
2. Batenin V.M., Buchanov V.V., et al. *Lazery na samoogranichennykh perekhodakh atomov metallov* (Self-Contained Metal Atom Lasers) (Moscow: Nauchnaya kniga, 1998).
3. Huang Z.G., Namba J., Shimizu F. *Jpn. J. Apll. Phys.*, **25**, 1677 (1986).
4. Withford M.J., Brown D.J.W., Piper J.A. *Opt. Commun.*, **110**, 699 (1994).
5. Astadjov D.N., Sabotinov N.V., Vuchkov N.K. *Opt. Commun.*, **56**, 279 (1985).
6. Astadjov D.N., Sabotinov N.V., Vuchkov N.K. *IEEE J. Quantum Electron.*, **24**, 1927 (1988).
7. Astadjov D.N., Isaev A.A., Petrash G.G., Ponomarev I.V., Sabotinov N.V., Vuchkov N.K. *IEEE J. Quantum. Electron.*, **28**, 1966 (1992).
8. Sabotinov N.V., Vuchkov N.K., Astadjov D.N. *Opt. Commun.*, **95**, 55 (1993).
9. Carman R.J., Mildren R.P., Withford M.J., Brown D.J.W., Piper J.A. *IEEE J. Quantum. Electron.*, **36**, 438 (2000).
10. Cheng C., Sun W. *Opt. Commun.*, **144**, 109 (1997).
11. Ivanov V.V., Klopovskii K.S., Mankelevich Yu.A., Motovilov S.A., et al. *Proc. SPIE Int. Soc. Opt. Eng.*, **4747**, 128 (2002).
12. Boichenko A.M., Yakovlenko S.I. *Kvantovaya Elektron.*, **32**, 172 (2002) [*Quantum Electron.*, **32**, 172 (2002)].
13. Boichenko A.M., Yakovlenko S.I. *Laser Phys.*, **12**, 1007 (2002).
14. Boichenko A.M., Tarasenko V.F., Yakovlenko S.I. *Laser Phys.*, **10**, 1159 (2000).
15. Yakovlenko S.I. (Ed.) *Trudy IOFAN*, **21** (1989).
16. Bokhan P.A. *Doct. Diss.* (Novosibirsk, Institute of Atmospheric Optics, Siberian Branch, Russian Academy of Sciences, 1988).
17. Carman R.J., Mildren R.P., Withford M.J., Brown D.J.W., Piper J.A. *Opt. Commun.*, **157**, 99 (1998).
18. Yakovlenko S.I. *Kvantovaya Elektron.*, **30**, 501 (2000) [*Quantum Electron.*, **30**, 501 (2000)].
19. Boichenko A.M., Evtushenko G.S., Yakovlenko S.I., Zhdaneev O.V. *Laser Phys.*, **11**, 580 (2001).
20. Mildren R.P., Withford M.J., Brown D.J.W., Carman R.J., Piper J.A. *IEEE J. Quantum. Electron.*, **34**, 2275 (1998).
21. Hayashi K., Iseki Y., Suziki S., Watanabe I., Noda E., Morimiya O. *Jpn. J. Appl. Phys.*, **31**, L1689 (1992).
22. Garcia-Prieto J., Ruz M.E., Poulain E., Ozin G.A., Novaro O. *J. Chem. Phys.*, **81**, 5920 (1984).
23. Carman R.J., Mildren R.P., Piper J.A., Marshal G.D., Coutts D.W. *Proc. SPIE Int. Soc. Opt. Eng.*, **4184**, 215 (2001).
24. Boichenko A.M., Tarasenko V.F., Fedeneev A.V., Yakovlenko S.I. *Kvantovaya Elektron.*, **24**, 697 (1997) [*Quantum Electron.*, **27**, 679 (1997)].
25. Petrash G.G. *Laser Phys.*, **10**, 994 (2000).
26. Gudzenko L.I., Yakovlenko S.I. *Plazmennye lazery* (Plasma Lasers) (Moscow: Atomizdat, 1978).
27. Kushner M.J., Warner B.E. *J. Appl. Phys.*, **54**, 2970 (1983).
28. Soldatov A.N., Fedorov V.F. *Izv. Vyssh. Uchebn. Zaved., Ser. Fiz.*, **26** (9), 80 (1983).
29. Evtushenko G.S., Petrash G.G., Sukhanov V.B., Fedorov V.F. *Kvantovaya Elektron.*, **28**, 220 (1999) [*Quantum Electron.*, **29**, 775 (1999)].
30. Evtushenko G.S. et al. *Opt. Atmos. Okean.*, **13**, 254 (2000).
31. Smirnov B.M. *Iony i vozbuzhdennye atomy v plazme* (Ions and Excited Atoms in Plasma) (Moscow: Nauka, 1974).
32. Lotz W. *Astrophysic. J. Suppl.*, **15**, 207 (1967).
33. Mewe R. *Astronomy and Astrophys.*, **20**, 265 (1972).
34. Phelps A.V. *J. Phys. Chem. Refer. Data*, **19**, 656 (1990).
35. *Fizika ion-ionnykh i elektron-ionnykh stolknovenii* (Physics of Ion–Ion and Electron–Ion Collisions) (Moscow: Mir, 1986).
36. Dautov N.G., Starik A.M. *TVT*, **31**, 292 (1993).
37. Johnson R., Bionoli M. *J. Chem. Phys.*, **61**, 2112 (1974).
38. *Neravnovesnaya kolebatel'naya kinetika* (Nonequilibrium Vibrational Kinetics) (Moscow: Mir, 1989).
39. Gross R.W., Bott J.F. (Eds) *Handbook of Chemical Lasers* (New York: Wiley, 1980; Moscow: Mir, 1980).
40. Mazevet S., et al. *J. Phys. B*, **32**, 1269 (1999).
41. Gallup G.A., Xu Y., Fabrikant I.I. *Phys. Rev. A*, **57**, 2596 (1998).
42. Thomson J. *Phil. Mag. S.6*, **47** (278), 337 (1924).
43. McDaniel E.W. *Collision Phenomena in Ionized Gases* (New York: Wiley, 1964).